International Journal of Automation and Computing 7(3), August 2010, 349-358
DOI: 10.1007/s11633-010-0514-8

Modelling and Remote Control of an Excavator

Yang Liu[1, 2] Mohammad Shahidul Hasan[1] Hong-Nian Yu[1]

[1]Faculty of Computing, Engineering and Technology, Staffordshire University, Stafford ST18 0AD, UK

[2]Centre for Applied Dynamics Research, School of Engineering, University of Aberdeen, Aberdeen AB24 3UE, UK

Abstract: This paper presents the results of an on-going project and investigates modelling and remote control issues of an industry excavator. The details of modelling, communication, and control of a remotely controllable excavator are studied. The paper mainly focuses on trajectory tracking control of the excavator base and robust control of the excavator arm. These will provide the fundamental base for our next research step. In addition, extensive simulation results for trajectory tracking of the excavator base and robust control of the excavator arm are given. Finally, conclusions and further work have been identified.

Keywords: Excavator, remote control, mechatronics, modelling.

1 Introduction

The remote control of an excavator plays a significant role in real-life applications, such as nuclear decommissioning, building demolition, military operations, rescue missions, etc. The advantage of remote control is that it allows the operator to control the machine in a remote safe environment via the wired/wireless network. In order to carry out a specific task, there are two subtasks for an excavator. First, the excavator has to find a feasible path from its initial location to the destination. Second, a robust control approach has to be designed to execute the desired excavation tasks. According to these requirements, we proposed a framework of remote control of an excavator in [1]. This paper further expands that work in the following aspects: 1) modelling of the excavator base, 2) control of the excavator base, 3) robust control of the excavator arm, and 4) remote control of the excavator base.

Based on the earlier work, implementation of a remote-control excavator mainly focused on modelling and control of the machine. The modelling work includes kinematic[2] and dynamic[3] modelling, modelling of interaction between the machine and the environment[4], and parameter identification[5−7]. The key reason for modelling and parameter identification during the digging operation is to provide online parameters for the real-time monitoring and remote control. In [5], a novel approach for experimental determination of the joint parameters and friction coefficients was developed on the excavator arm. Zweiri[6] presented another robust, fast, and simple technique for the experimental identification of the joint parameters and friction coefficients of a full-scale excavator arm. Furthermore, an online soil parameter estimation scheme was proposed in [7]. During the earlier stage of excavation control, impedance control was considered as a prevalent robust control approach to achieve compliant motion in contact tasks. In [8], a position-based impedance controller was presented on various contact experiments by using an instrumented mini-excavator. Details of robust impedance control for a hydraulic excavator have been presented in [9, 10].

In contrast to control of the excavator arm, motion control, and path planning for the excavator base have also been studied in a number of research papers[11,12]. In [13], a vision-based control system for a tracked excavator was presented. The system includes several controllers that collaborate to move the excavator from a starting position to a goal position. Furthermore, a number of researchers have investigated the feasibility of remote-control excavation. Many of these studies have addressed the possible use of the remote control approach on the excavator[1, 8]. However, in a remote-control excavator system, if the operator cannot sense the condition of contact, the work efficiency will decrease in comparison to direct control by the human operator. Therefore, the design of the joystick with proper force feedback[14, 15] is key to controlling an excavator remotely. The joystick can make skilful operators adapt their operations to the excavating environment based on their empirical knowledge, and can further realize efficient excavation. Moreover, in contrast to controlling a real hydraulic excavator, there are many studies that implement their work on the virtual excavator[16, 17]. The virtual excavator system appears to be a low-cost, safe, and reliable system that can be used to test both the system and the control strategy in a virtual environment.

As discussed above, many research studies have focused on the modelling and controller development stages, but there are few researches studying the remote operations from a network communication point of view. Furthermore, it is found that the efficiency of excavation by a human operator[18] is a notable issue that has potential commercial value. On the other hand, a remote-control excavator has been the wish of both industry and manufacturing over the past two decades. Much of the work on terrestrial excavation has focused on tele-operation, rather than on the system requirements for autonomous operation. However, although remarkable and valuable progress has been made on automated excavation, the remote control of a full-scale excavator has not been commercially demonstrated.

In this paper, we will report the further development based on the work in [1] and will focus on the work from the following aspects: 1) trajectory tracking control of the excavator base, and 2) robust control of the excavator arm. Section 2 studies the models of the excavator base and the excavator arm. Those models will provide the basis

Manuscript received August 23, 2009; revised November 18, 2009

for the system design, development of the controllers, task/path planning, simulation, and validation, etc. Section 3 investigates the control approaches for controlling the excavator base and the excavator arm. Section 4 proposes a wireless networked control scheme for the excavator base. Finally, the conclusions and future work are given in Section 5.

Notation.

1) Parameters of the excavator base model:

$M = 10\,\text{kg}$: Mass of the entire base.

$I_A = 1.0\,\text{kg·m}^2$: Moment of inertia of the entire base considering point A.

$I_0 = 0.001\,\text{kg·m}^2$: Moment of inertia of the wheel complex.

$L = 0.35\,\text{m}$: Width of the base.

$r = 0.035\,\text{m}$: Radius of the wheels.

$d = 0.05\,\text{m}$: Distance between point A and C.

θ_c: Angle representing the orientation of the base.

θ_R: Angle position of the right wheel.

θ_L: Angle position of the left wheel.

τ_R: Actuation torque of the right wheel.

τ_L: Actuation torque of the left wheel.

2) Parameters of the excavator arm model:

$M_{\text{bo}} = 1566\,\text{kg}$: Mass of boom.

$M_{\text{st}} = 735\,\text{kg}$: Mass of stick.

$M_{\text{bu}} = 432\,\text{kg}$: Mass of bucket.

$M_{\text{load}} = 500\,\text{kg}$: Mass of load.

$\text{V}_b = 0.58\,\text{m}^3$: Volume of bucket.

$\rho = 1921.8\,\text{kg/m}^3$: Soil density.

$M_{\max} = V_b \cdot \rho$: Maximal load weight.

$I_{\text{bo}} = 14250.6\,\text{kg·m}^2$: Moment of inertia of boom.

$I_{\text{st}} = 727.7\,\text{kg·m}^2$: Moment of inertia of stick.

$I_{\text{bu}} = 224.6\,\text{kg·m}^2$: Moment of inertia of bucket.

θ_1 : Angle of base.

θ_2 : Angle of boom.

θ_3 : Angle of stick.

θ_4 : Angle of bucket.

θ_b: Angle between bucket bottom and x_4-axis.

θ_{dg}: Angle between bucket edge and horizontal line.

$a_1 = 0.05\,\text{m}$: O_0O_1.

$a_2 = 5.16\,\text{m}$: O_1O_2.

$a_3 = 2.59\,\text{m}$: O_2O_3.

$a_4 = 1.33\,\text{m}$: O_3O_4.

$r_2 = 2.71\,\text{m}$: O_1G_2.

$r_3 = 0.64\,\text{m}$: O_2G_3.

$r_4 = 0.65\,\text{m}$: O_3G_4.

$\alpha_2 = 0.2566\,\text{rad}$: $\angle G_2O_1O_2$.

$\alpha_3 = 0.3316\,\text{rad}$: $\angle G_3O_2O_3$.

$\alpha_4 = 0.3944\,\text{rad}$: $\angle G_4O_3O_4$.

B_{bo}: Viscous friction coefficient of boom.

B_{st}: Viscous friction coefficient of stick.

B_{bu}: Viscous friction coefficient of bucket.

$g = 9.81\,\text{N/kg}$: Acceleration due to gravity.

$T_s = 10\,\text{ms}$: Sampling time.

2 Modelling of an excavator

2.1 Modelling of the excavator base

The excavator base model is taken from [19, 20]. It has two driving wheels and a free rotating front wheel. Two wheels are independently driven by actuators to produce transition and orientation. The excavator base model is shown in Fig. 1, and the parameters are given in notations. The centre of mass and the centre of the excavator base gear are represented by points C and A, respectively.

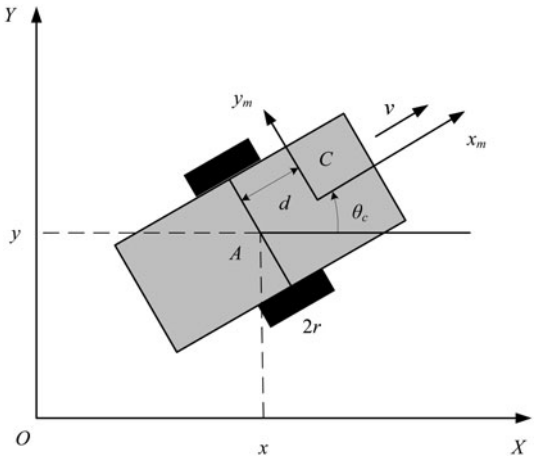

Fig. 1 The excavator base model for position control given in [19, 20]

The kinematic model of the excavator base is presented as shown below:

$$\dot{x}_A = \frac{r}{2}(\dot{\theta}_R + \dot{\theta}_L)\cos\theta \tag{1}$$

$$\dot{y}_A = \frac{r}{2}(\dot{\theta}_R + \dot{\theta}_L)\sin\theta \tag{2}$$

$$\dot{\theta}_c = \frac{r(\dot{\theta}_R - \dot{\theta}_L)}{2R}. \tag{3}$$

The dynamic model of the excavator base is expressed as follows:

$$D_c\ddot{q} + C_c\dot{q} = \tau_c \tag{4}$$

where

$$q = \begin{bmatrix} \theta_R \\ \theta_L \end{bmatrix}, \quad D_c = \begin{bmatrix} A & B \\ B & A \end{bmatrix},$$

$$C_c = \begin{bmatrix} 0 & K \\ K & 0 \end{bmatrix}, \quad \tau_c = \begin{bmatrix} \tau_R \\ \tau_L \end{bmatrix},$$

$$A = \frac{Mr^2}{4} + \frac{(I_A + Md^2)r^2}{4R^2} + I_0$$

$$B = \frac{Mr^2}{4} - \frac{(I_A + Md^2)r^2}{4R^2}$$

and $K = A/2$.

2.2 Modelling of the excavator arm

The dynamic model of the excavator can be expressed concisely using the form of the well-known rigid-link manipulator equations of motion[21]:

$$D_a(\theta)\ddot{\theta} + C_a(\theta,\dot{\theta})\dot{\theta} + G_a(\theta) + B_a(\dot{\theta}) = \Gamma\tau_a - F_L \tag{5}$$

where $\theta = [\theta_1 \;\; \theta_2 \;\; \theta_3 \;\; \theta_4]^{\text{T}}$ is the vector of measured joint angles as defined in Fig. 2; $D_a(\theta)$ represents inertia; $C_a(\theta,\dot{\theta})$ represents Coriolis and centripetal effects; $G_a(\theta)$ represents gravity forces; $B_a(\dot{\theta})$ represents frictions; Γ is the corresponding input matrix; vector $\tau_a = [\tau_1 \;\; \tau_2 \;\; \tau_3 \;\; \tau_4]^{\text{T}}$ specifies the torques acting on the joint shafts; and F_L represents the

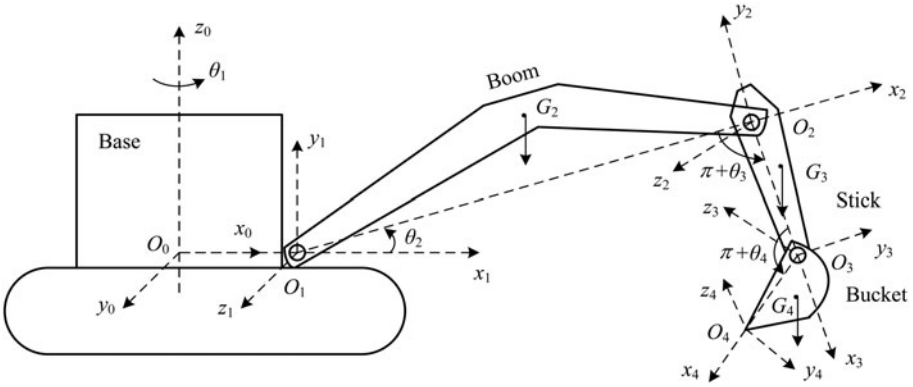

Fig. 2 Schematic diagram of an excavator[4]

interactive torques between the bucket and the environment during the digging operation.

According to [4], $D_a(\theta)$, $C_a(\theta,\dot{\theta})$, $G_a(\theta)$, Γ, and F_L are given by the following expression:

$$D_a(\theta)=\begin{bmatrix} D_{11} & D_{12} & D_{13} & D_{14} \\ D_{21} & D_{22} & D_{23} & D_{24} \\ D_{31} & D_{32} & D_{33} & D_{34} \\ D_{41} & D_{42} & D_{43} & D_{44} \end{bmatrix} \tag{6}$$

where

$$\begin{aligned}
D_{44} &= I_{\mathrm{bu}} + M_{\mathrm{bu}}R_4^2 \\
D_{33} &= D_{44} + I_{\mathrm{st}} + M_{\mathrm{st}}r_3^2 + M_{\mathrm{bu}}[a_3^2 + 2a_3r_4\cos(\theta_4+\alpha_4)] \\
D_{22} &= D_{33} + I_{\mathrm{bo}} + M_{\mathrm{bo}}r_2^2 + M_{\mathrm{st}}[a_2^2 + 2a_2r_3\cos(\theta_3+\alpha_3)] + \\
&\quad M_{\mathrm{bu}}[a_2^2 + 2a_2a_3c_3 + 2a_2r_4\cos(\theta_{34}+\alpha_4)] \\
D_{34} &= D_{43} = D_{44} + M_{\mathrm{bu}}a_3r_4\cos(\theta_4+\alpha_4) \\
D_{24} &= D_{42} + D_{34} + M_{\mathrm{bu}}a_2r_4\cos(\theta_{34}+\alpha_4) \\
D_{23} &= D_{32} = D_{24} + I_{\mathrm{st}} + M_{\mathrm{st}}[r_3^2 + a_2r_3\cos(\theta_3+\alpha_3)] + \\
&\quad M_{\mathrm{bu}}[a_3^2 + a_2a_3c_3 + a_3\cos(\theta_4+\alpha_4)]
\end{aligned}$$

$$C_a(\theta,\dot{\theta})=\begin{bmatrix} C_{11} & C_{12} & C_{13} & C_{14} \\ C_{21} & C_{22} & C_{23} & C_{24} \\ C_{31} & C_{32} & C_{33} & C_{34} \\ C_{41} & C_{42} & C_{43} & C_{44} \end{bmatrix} \tag{7}$$

where

$$\begin{aligned}
C_{22} &= -M_{\mathrm{st}}a_2r_3\dot{\theta}_{23}\sin(\theta_3+\alpha_3) - M_{\mathrm{bu}}a_2a_3\dot{\theta}_{23}s_3 - \\
&\quad M_{\mathrm{bu}}a_2r_4\dot{\theta}_{234}\sin(\theta_{34}+\alpha_4) \\
C_{23} &= -M_{\mathrm{st}}a_2r_3\dot{\theta}_{23}\sin(\theta_3+\alpha_3) - M_{\mathrm{bu}}a_2a_3\dot{\theta}_{23}s_3 - \\
&\quad M_{\mathrm{bu}}a_2r_4\dot{\theta}_{234}\sin(\theta_{34}+\alpha_4) \\
C_{24} &= -M_{\mathrm{bu}}a_2r_4\dot{\theta}_{234}\sin(\theta_{34}+\alpha_4) \\
C_{32} &= a_2\dot{\theta}_2[M_{\mathrm{bu}}a_3s_3 + M_{\mathrm{st}}r_3\sin(\theta_3+\alpha_3)] - \\
&\quad M_{\mathrm{bu}}a_3r_4\dot{\theta}_{234}\sin(\theta_4+\alpha_4) \\
C_{33} &= -M_{\mathrm{bu}}a_3r_4\dot{\theta}_{234}\sin(\theta_4+\alpha_4) \\
C_{34} &= -M_{\mathrm{bu}}a_3r_4\dot{\theta}_{234}\sin(\theta_4+\alpha_4) \\
C_{42} &= M_{\mathrm{bu}}r_4\dot{\theta}_2[a_2\sin(\theta_{34}+\alpha_4) + a_3\sin(\theta_4+\alpha_4)] + \\
&\quad M_{\mathrm{bu}}a_3r_4\dot{\theta}_3\sin(\theta_4+\alpha_4) \\
C_{43} &= M_{\mathrm{bu}}a_3r_4\sin(\theta_4+\alpha_4) \\
C_{44} &= 0
\end{aligned}$$

$$G_a(\theta)=[G_1 \;\; G_2 \;\; G_3 \;\; G_4]^{\mathrm{T}} \tag{8}$$

where

$$\begin{aligned}
G_2 &= (M_{\mathrm{bu}}+M_{\mathrm{st}})ga_2c_2 + M_{\mathrm{bo}}gr_2\cos(\theta_2+\alpha_2) \\
G_3 &= M_{\mathrm{bu}}ga_3c_{23} + M_{\mathrm{st}}gr_3\cos(\theta_{23}+\alpha_3) \\
G_4 &= M_{\mathrm{bu}}gr_4\cos(\theta_{234}+\alpha_4)
\end{aligned}$$

$$B_a(\dot{\theta})=\left[B_{\mathrm{ba}}\dot{\theta}_1 \;\; B_{\mathrm{bo}}\dot{\theta}_2 \;\; B_{\mathrm{st}}\dot{\theta}_3 \;\; B_{\mathrm{bu}}\dot{\theta}_4\right]^{\mathrm{T}} \tag{9}$$

$$\Gamma=\begin{bmatrix} \Gamma_{11} & \Gamma_{12} & \Gamma_{13} & \Gamma_{14} \\ \Gamma_{21} & 1 & -1 & 0 \\ \Gamma_{31} & 0 & 1 & -1 \\ \Gamma_{41} & 0 & 0 & 1 \end{bmatrix}. \tag{10}$$

The interaction between the excavator bucket and the environment is presented in Fig. 3.

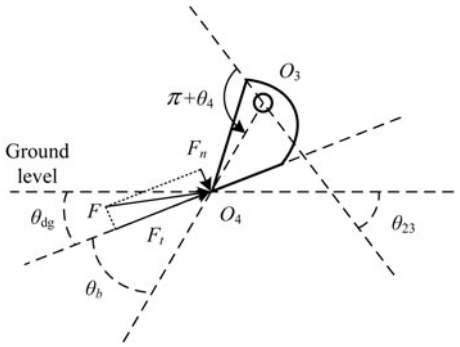

Fig. 3 The interaction between the excavator bucket and the environment[4]

According to [22], F_t and F_n are the tangential and normal components of the soil reaction force at the bucket, respectively. The tangential component can be calculated as

$$F_t = k_1bh \tag{11}$$

where k_1 is the specific digging force in $\mathrm{N/m^2}$, and h and b are the thickness and width of the cut slice of soil. The normal component F_n is calculated as

$$F_n = \Psi F_t \tag{12}$$

where $\Psi = 0.1 - 0.45$ is a dimensionless factor that depends on the digging angle, digging conditions, and the wear of the cutting edge.

Therefore, according to Fig. 3, the loading torque is given as shown below:

$$F_L = \begin{bmatrix} \tau_b \\ a_2[F_t \sin(\theta_2 - \theta_{\mathrm{dg}}) - F_n \cos(\theta_2 - \theta_{\mathrm{dg}})] \\ a_3[F_t \sin(\theta_{23} + \theta_{\mathrm{dg}}) - F_n \cos(\theta_{23} + \theta_{\mathrm{dg}})] \\ -a_4(F_t \sin\theta_b + F_n \cos\theta_b) \end{bmatrix}. \tag{13}$$

Since this paper concerns mainly on the motion control, the elements D_{1i}, D_{i1}, C_{1i}, C_{i1}, Γ_{1i}, Γ_{i1} (i = 1, 2, 3, and 4), G_1, B_{ba}, τ_1, and τ_b are not used in the proposed control law. However, those parameters are important in the forced control and will be investigated in future work.

3 Control of an excavator

3.1 Control of the excavator base

Two proportional-derivative (PD) controllers have been implemented and tuned, as suggested in [19, 20]. Equations (14)–(19) are used to control the right and left wheel actuator torques. The gains of the applied PD controllers are given in Table 1.

$$e_v(t) = v_{\mathrm{ref}}(t) - v(t) = u_1 - v(t) \tag{14}$$

$$e_\omega(t) = \omega_{\mathrm{ref}}(t) - \omega(t) = u_2 - \omega(t) \tag{15}$$

$$u_v(t) = K_{pv} e_v(t) + K_{iv} \int e_v(t)\mathrm{d}(t) \tag{16}$$

$$u_\omega(t) = K_{p\omega} e_\omega(t) + K_{i\omega} \int e_\omega(t)\mathrm{d}(t) \tag{17}$$

$$u_R(t) = \tau_R = \frac{1}{2}u_v(t) + \frac{1}{2}u_\omega(t) \tag{18}$$

$$u_L(t) = \tau_L = \frac{1}{2}u_v(t) - \frac{1}{2}u_\omega(t). \tag{19}$$

Table 1 Parameters of PD controllers for wheel torque control of the excavator base model given in [19, 20]

Parameters	Descriptions	Values
K_{pv}	The proportional component for the forward speed control	6.48
K_{iv}	The integral component for the forward speed control	56.9098
$K_{p\omega}$	The proportional component for the turning speed control	2.05
$K_{i\omega}$	The integral component for the turning speed control	8.4803

The extended backstepping position controller that was proposed in [20] is used in the outer loop for position control. The position controller outputs are defined by (20)–(22), where the parameter values are given in Table 2.

$$\begin{bmatrix} e_1 \\ e_2 \\ e_3 \end{bmatrix} = \begin{bmatrix} \cos\theta_c & \sin\theta_c & 0 \\ -\sin\theta_c & \cos\theta_c & 0 \\ 0 & 0 & 1 \end{bmatrix} \begin{bmatrix} x_r - x \\ y_r - y \\ \theta_r - \theta_c \end{bmatrix} \tag{20}$$

$$u_1 = v_r \cos e_3 + \frac{k_1 e_1}{\sqrt{k_4 + e_1^2 + e_2^2}} \tag{21}$$

$$u_2 = \omega_r + \frac{k_2 v_r e_2}{\sqrt{k_5 + e_1^2 + e_2^2}} + \frac{k_3 v_r \sin e_3}{\sqrt{k_6 + e_3^2}}. \tag{22}$$

Table 2 Parameters of the backstepping position control of the excavator base model given in [20]

Parameters	Values
k_1	18.2620
k_2	18.75
k_3	9.8229
k_4	26.5370
k_5	1.0164
k_6	2.0028

3.2 Robust control of the excavator arm

Usually, the excavator is required to carry out tasks involving contact with its environment, such as levelling and digging. Toward autonomous excavation, it is necessary to develop a controller that is robust to uncertainties associated with such tasks.

Although there are some pronounced differences between the classical robot manipulator and robotic excavation, there are also some parallels. Therefore, many control approaches that have been developed for the robot manipulator can be adopted by the robotic excavation. In this section, we will first study the control of the excavator using the conventional computed torque control that has been developed on the fully actuated robot manipulator. Then, we will develop a robust control approach that is effective to reject external disturbance during excavation. After that, extensive simulation results will be compared.

Using the dynamic model of the excavator arm in (5), the computed torque control (CTC) law is given as shown below:

$$U_a = \hat{D}_a(\theta)\dot{\theta}_v + \hat{C}_a(\theta, \dot{\theta})\dot{\theta} + \hat{G}_a(\theta) + \hat{B}_a(\dot{\theta}) \tag{23}$$

where $\dot{\theta}_v = \ddot{\theta}_d - k_v \dot{e}_a - k_p e_a$; $e_a = \theta - \theta_d$; k_v and k_p are linear gains to be designed; $\hat{D}_a(\theta)$ is the estimated inertia; $\hat{C}_a(\theta, \dot{\theta})$ is the estimated Coriolis and centripetal effect; $\hat{G}_a(\theta)$ is the estimated gravity forces; $\hat{B}_a(\dot{\theta})$ is the estimated friction effect, U_a is the computed torques applied to the system, θ_d, $\dot{\theta}_d$, and $\ddot{\theta}_d$ are the desired joint link angle, angular velocity, and angular acceleration, respectively.

It is found that the CTC approach is specified by the inverse dynamics of the excavator (5). The controller (23) generates the generalized torques to be applied to the excavator producing the desired motion. The simulation is carried out in two cases: 1) tracking the desired motion without payload and 2) tracking the desired motion with payload ($M_{\mathrm{load}} = 500\,\mathrm{kg}$) but it is assumed to be unknown. For both cases, the linear gains $k_v = 100$ and $k_p = 150$ are used.

The simulation results are presented as follows. In Fig. 4, the actual bucket motion under the CTC law without payload is shown. To analyze the performance of the CTC law, Figs. 5 and 6 present the tracking errors of the bucket and the bucket head, respectively. The tracking error is the absolute distance from the actual trajectory to the desired trajectory. In Fig. 5, it can be seen that the case with unknown payload gives a maximal tracking error that is about 0.056 m, and the average tracking error with payload is apparently larger than the case without payload. Also, in Fig. 6, the tracking performance is not as good as desired when the system is loaded with unknown payload. In Fig. 7, the control inputs by using the CTC law with payload are given.

From the simulation results above, it can be found that the CTC law cannot give a desired tracking performance under the case of unknown payload. Therefore, a robust control approach is required to adapt to an uncertain circumstance. According to the dynamic model in (5), the robust control (RC) law[21] is introduced as shown below:

$$\tilde{x}(t) = [\dot{e}(t) \quad e(t)]^{\mathrm{T}} \tag{24}$$

$$\bar{W}\Theta(t) + \bar{W}_0(t) = D(\theta)\{\dot{v} - \mu(\dot{e} + P_{12}e)\} + C(\theta, \dot{\theta})v + G(\theta) \tag{25}$$

$$T(t) = T_f(t) + T_1(t) \tag{26}$$

$$T_1(t) = -(P_{11} + P_{cc}\Gamma^{-1}P_{cc})P_1\tilde{x}(t) + P_{cc}e(t) \tag{27}$$

$$T_f(t) = \bar{W}(t)\Theta_v(t) + \bar{W}_0(t) \tag{28}$$

$$\Theta_v(t) = -F_1(t)\bar{\Theta}\bar{\theta}_i \geqslant \theta, \quad \forall i \tag{29}$$

$$F_1(t) = \mathrm{diag}\{\mathrm{sign}(f_1), \mathrm{sign}(f_2), \cdots, \mathrm{sign}(f_p)\} \tag{30}$$

$$F(t) = \tilde{x}^{\mathrm{T}}P^{\mathrm{T}}\bar{W}(t) = [f_1(t), f_2(t), \cdots, f_p(t)] \tag{31}$$

where $v = \dot{\theta}_d - P_{12}e$, Θ is a vector containing the unknown excavator and load parameters, which are known to lie in a bounded set: $\Omega = \left\{ \Theta \middle| |\theta_i| \leqslant \bar{\theta}_i, i = 1, 2, \cdots, p \right\}$, $\Theta_v(t)$ is a switching-function vector, P_{cc}, Γ, $P_{11} \in \mathbf{R}^{n\times n}$ are symmetric positive definite matrices, $P_{12} = P_{cc}^{-1}\Gamma$, and $P_1 = [I_{n\times n} \quad P_{12}]$.

In the simulation, the coefficients are chosen as $P_{cc} = 100I_{3\times3}$, $P_{11} = 80I_{3\times3}$, $P_{12} = 40I_{3\times3}$, and $\mu = 3.5$. The resulting linear feedback control law is

$$T_1(t) = -82.5\dot{e}(t) - 3200e(t). \tag{32}$$

The payload in the bucket is assumed unknown, but with known bounds, $0 \leqslant M_{\mathrm{load}} \leqslant M_{\max}$, where $M_{\max} = V_b \cdot \rho$ is the maximal weight that the excavator can load, V_b is the volume of the bucket, and ρ is the soil density. In the simulation, $M_{\mathrm{load}} = 500\,\mathrm{kg}$ and $M_{\max} = 1114.6\,\mathrm{kg}$. According to equations (28)–(31), the robust control law is given as shown below:

$$f(t) = [\{\dot{e}(t) + 40e(t)\}\bar{W}(t)] \tag{33}$$

$$\Theta_v(t) = -(M_{\mathrm{bu}} + M_{\max})\mathrm{sign}\{f(t)\} \tag{34}$$

$$T_f(t) = \bar{W}(t)\Theta_v(t) + \bar{W}_0(t). \tag{35}$$

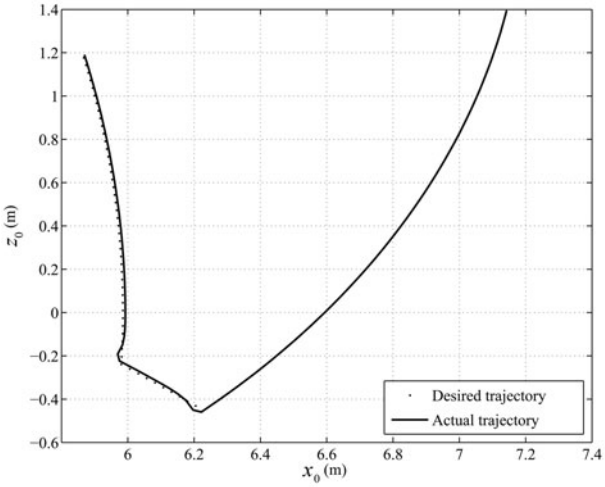

Fig. 4 The bucket (O_3) trajectory under the CTC law without payload

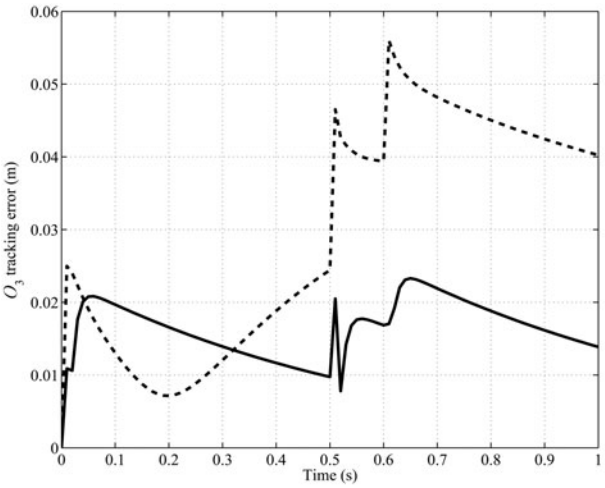

Fig. 5 The bucket (O_3) tracking errors (solid line: without payload; dash line: with unknown payload)

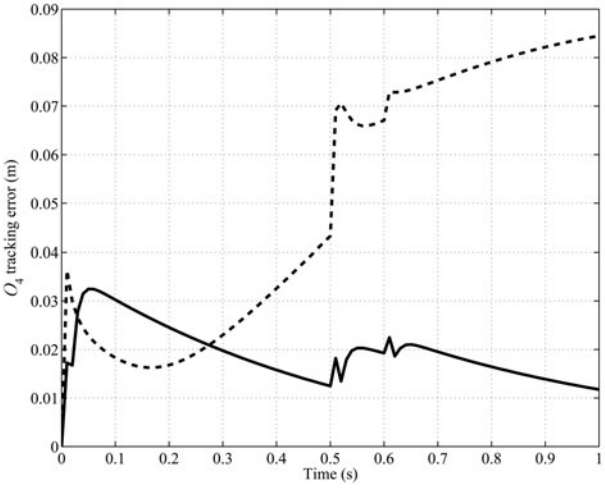

Fig. 6 The bucket head (O_4) tracking errors (solid line: without payload; dash line: with unknown payload)

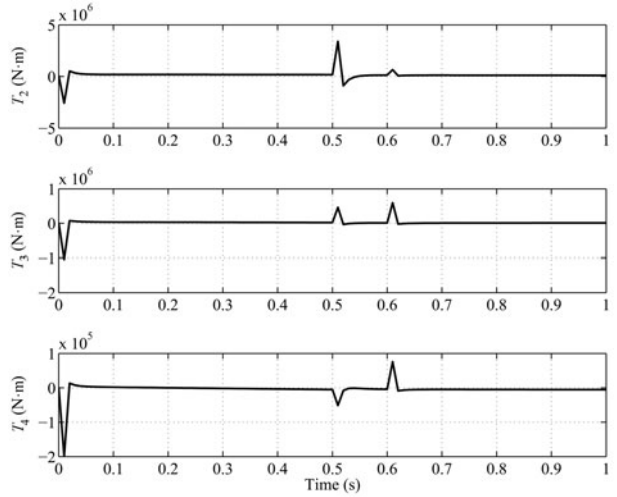

Fig. 7 The control torques under the CTC law with unknown payload

The comparison between the CTC law and the RC law is made by using the simulation results as follows. The tracking results of the desired bucket motion by using both control laws are presented in Fig. 8. For both simulations, the mass of the payload is assumed unknown for the controller design. As shown in Fig. 8, it can be seen that the CTC law gives a maximal tracking error about 0.056 m, while the RC law gives a better tracking performance, i.e., the average tracking errors given by the RC law is obviously less than the average tracking errors given by the CTC law. In Fig. 9, it can be found that the tracking results are consistent with the results shown in Fig. 8. Although the RC law gives a large tracking error at the beginning, the error becomes smaller finally. Therefore, the comparison can validate that the RC law is more effective and more robust to an uncertain circumstance. Furthermore, the control torques by using the CTC law and the RC law are compared in Fig. 10. From this figure, it can be found that the control inputs of the RC law are much larger than the control inputs of the CTC law. It gives a reasonable result that the RC law effectively reduces the tracking error during the excavation, and gives a better tracking performance.

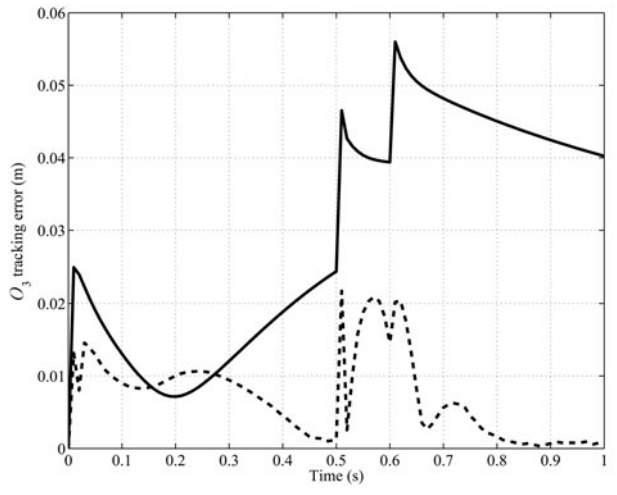

Fig. 8 The bucket ($O3$) tracking errors with unknown payload (solid line: the CTC law; dash line: the RC law)

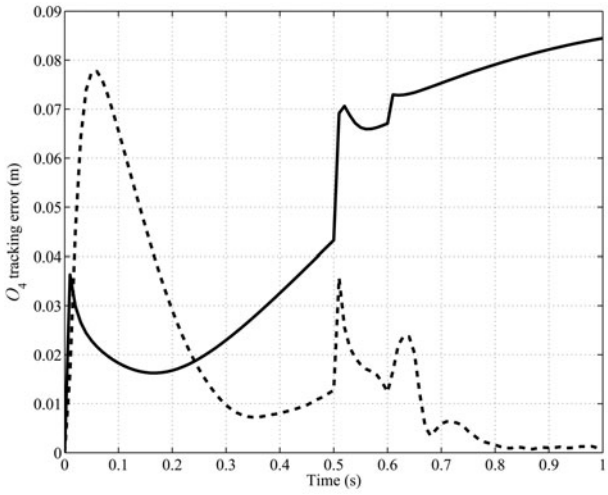

Fig. 9 The bucket head (O_4) tracking errors with unknown payload (solid line: the CTC law; dash line: the RC law)

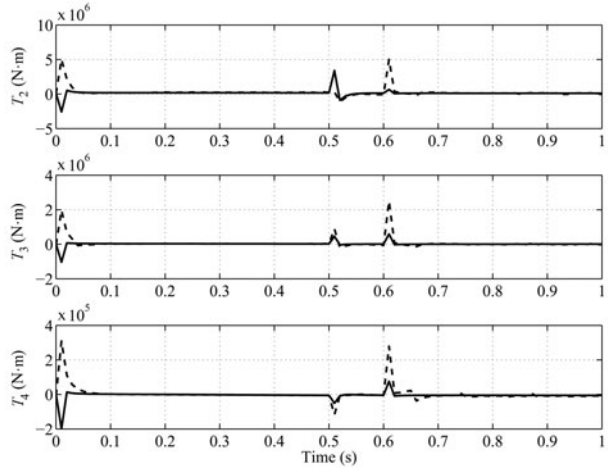

Fig. 10 The control torques with unknown payload (solid line: the CTC law; dash line: the RC law)

4 Remote control of the excavator base

The co-simulation framework[23,24] that utilizes Matlab Simulink to model the plant-controller and OPNET to simulate the network has been used to implement the position control of the excavator base and is shown in Fig. 11. The co-simulation parameters are given in Table 3.

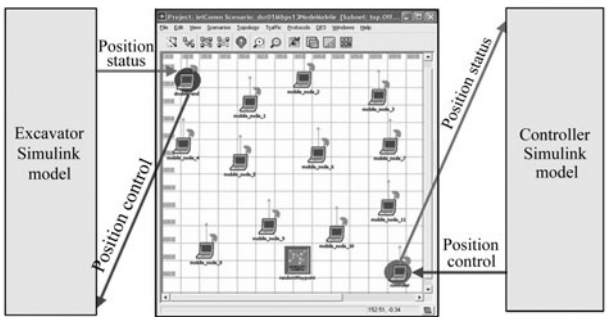

Fig. 11 Interactive Simulink-OPNET co-simulation

Table 3 Parameters of Simulink-OPNET co-simulation for the excavator base position control given in [19, 20]

Parameters	Values
Simulation area	174 m × 174 m
Number of nodes	13
Wireless communication standard	The IEEE 802.11b (direct sequence)
Signal propagation model	The pass loss and the fading[25, 26]
Mobile ad-hoc network (MANET) routing protocol	The dynamic source routing (DSR) protocol[27, 28]
Media access control (MAC) protocol	The carrier sense multiple access with collision avoidance (the CSMA/CA)[29]
Packet size	98 bytes
Data rate	11 Mbps[30]
Wireless card	The Lucent ORiNOCO wireless network card[30]
Wireless card output power	15 dBm[30]
Wireless card reception sensitivity	−82 dBm (11 Mbps)[30]
Connection protocol	The user datagram protocol (UDP)[31−34]
Node movement model	The random way-point model[35, 36]
Sampling mechanism	Clock driven[34, 37−40]
Control mechanism	Event driven (upon the arrival of the state packet)[34, 37−40]
Actuation mechanism	Event driven (upon the arrival of the control packet)[34, 37−40]
Desired output	The reference x, y coordinates and orientation with time (see Fig. 12)
Sampling period	0.05 s [29, 41, 42]

The motive of position control is to control x and y coordinates, as well as the orientation. The desired x and y coordinate profiles and the orientation or direction are taken from [19] and are shown in Fig. 12 (a), (b), and Figs. 12 (c), respectively. The desired trajectory on x-y plane with time of the excavator base is depicted in Fig. 12 (d).

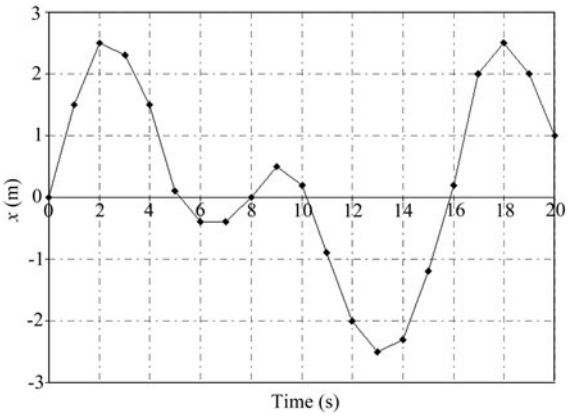

(a) Desired x coordinates

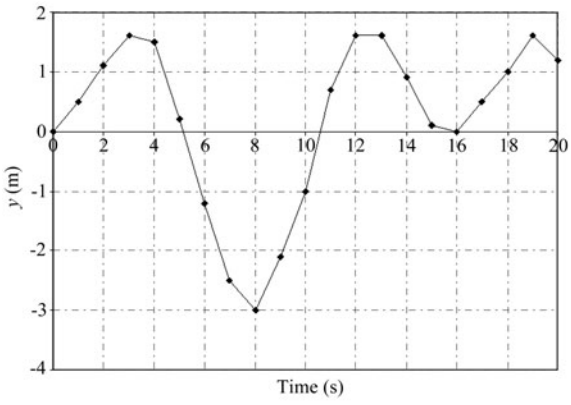

(b) Desired y coordinates

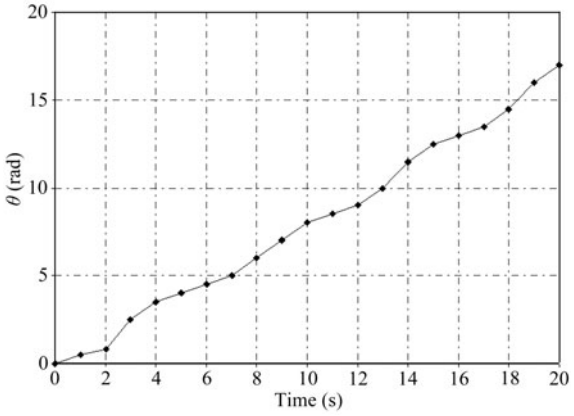

(c) Desired orientation

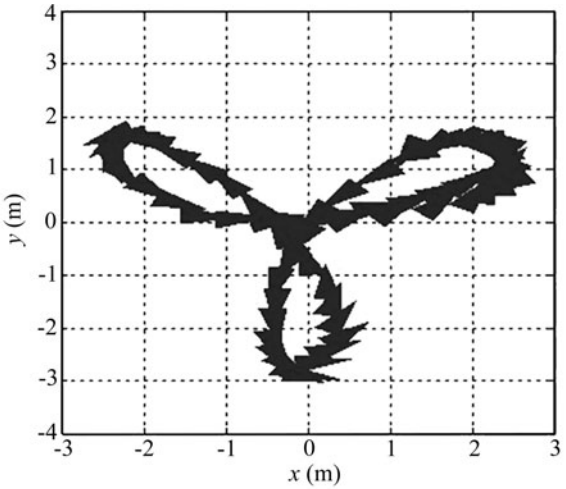

(d) Desired trajectory of the excavator base on x-y plane with time

Fig. 12 The desired x, y coordinates, orientation, and trajectory with time[19]

The excavator model sends x coordinate x, y coordinate y, and the orientation θ to the backstepping controller over

the OPNET MANET model. The controller compares the x, y, and θ values with the references $x_{\rm ref}$, $y_{\rm ref}$, and $\theta_{\rm ref}$ and sends the required inputs u_1 and u_2 to the velocity controller at the excavator site. The trajectory of the excavator base at the data rate of 11 Mbps is shown in Fig. 13. The control torques for the excavator right and left wheels are shown in Figs. 14 and 15, respectively.

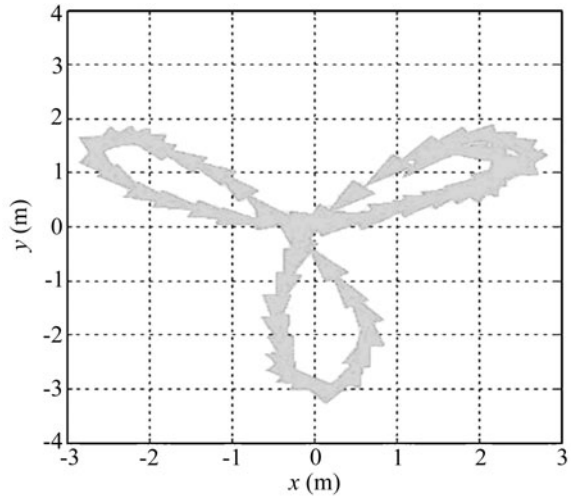

Fig. 13 Actual trajectories of the excavator base under various data rates

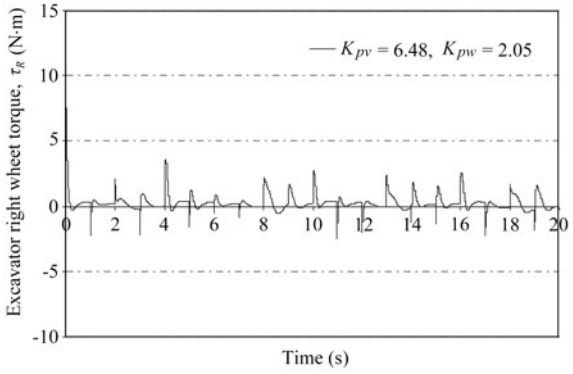

Fig. 14 The control torque of the excavator right wheel

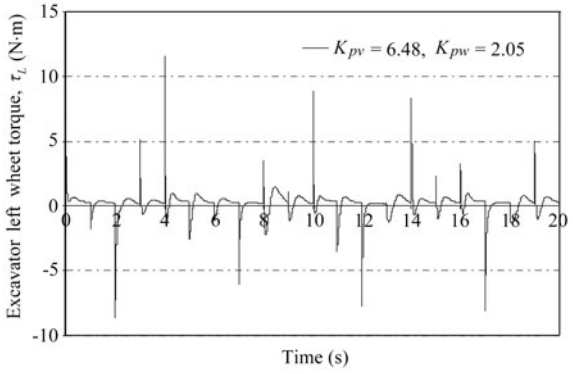

Fig. 15 The control torque of the excavator left wheel

5 Conclusions and future work

This paper has reported the work conducted in an ongoing project. The key issues in remotely controllable excavators have been identified. An overall architecture has been proposed and functions of each block of the architecture have been discussed. Some simulation work has been conducted to demonstrate the proposed system.

We will conduct further simulation on the whole system. The experimental study will also be investigated.

Acknowledgement

The authors thank Mr. Sam Wane for the useful discussion and J. C. Bamford Excavators Limited, Sellafield Limited for initiating this work.

References

[1] H. Yu, Y. Liu, M. S. Hasan. Review of modelling and remote control for excavators. *International Journal of Advanced Mechatronic Systems*, vol. 2, no. 1–2, pp. 68–80, 2009.

[2] A. J. Koivo. Kinematics of excavators (backhoes) for transferring surface material. *Journal of Aerospace Engineering*, vol. 7, no. 1, pp. 17–32, 1994.

[3] P. K. Vähä, M. J. Skibniewski. Dynamic model of excavator. *Journal of Aerospace Engineering*, vol. 6, no. 2, pp. 148–158, 1993.

[4] A. J. Koivo, M. Thoma, E. Kocaoglan, J. Andrade-Cetto. Modelling and control of excavator dynamics during digging operation. *Journal of Aerospace Engineering*, vol. 9, no. 1, pp. 10–18, 1996.

[5] S. Tafazoli, P. D. Lawrence, S. E. Salcudean. Identification of inertial and friction parameters for excavator arms. *IEEE Transactions on Robotics and Automation*, vol. 15, no. 5, pp. 966–971, 1999.

[6] Y. H. Zweiri. Identification schemes for unmanned excavator arm parameters. *International Journal Automation and Computing*, vol. 5, no. 2, pp. 185–192, 2008.

[7] C. P. Tan, Y. H. Zweiri, K. Althoefer, L. D. Seneviratne. Online soil parameter estimation scheme based on Newton-Raphson method for autonomous excavation. *IEEE/ASME Transactions on Mechatronics*, vol. 10, no. 2, pp. 221–229, 2005.

[8] S. Tafazoli, S. E. Salcudean, K. Hashtrudi-Zaad, P. D. Lawrence. Impedance control of a teleoperated excavator. *IEEE Transactions on Control Systems Technology*, vol. 10, no. 3, pp. 355–367, 2002.

[9] Z. Lu, A. A. Goldenberg. Robust impedance control and force regulation: Theory and experiment. *The International Journal of Robotics Research*, vol. 14, no. 3, pp. 225–254, 1995.

[10] Q. P. Ha, Q. H. Nguyen, D. C. Rye, H. F. Durrant-Whyte. Impedance control of a hydraulically-actuated robotic excavator. *Automation in Construction*, vol. 9, no. 5–6, pp. 421–435, 2000.

[11] L. E. Bernold. Motion and path control for robotic excavation. *Journal of Aerospace Engineering*, vol. 6, no. 1, pp. 1–18, 1993.

[12] S. Singh. Synthesis of Tactical Plans for Robotic Excavation, Ph. D. dissertation, The Robotics Institute, Carnegie Mellon University, Pittsburgh, PA, USA, 1995.

[13] P. Saeedi, P. D. Lawrence, D. G. Lowe, P. Jacobsen, D. Kusalovic, K. Ardron, P. H. Sorensen. An autonomous excavator with vision-based track-slippage control. *IEEE Transactions on Control Systems Technology*, vol. 13, no. 1, pp. 67–84, 2005.

[14] N. R. Parker, S. E. Salcudean, P. D. Lawrence. Application of force feedback to heavy duty hydraulic machines. In *Proceedings of IEEE Robotics and Automation Conference*, IEEE, Atlanta, USA, vol. 1, pp. 375–381, 1993.

[15] D. Kim, K. W. Oh, D. Hong, J. H. Park, S. H. Hong. Remote control of excavator with designed haptic device. In *Proceedings of International Conference on Control, Automation and Systems*, IEEE, Seoul, Korea, pp. 1830–1834, 2008.

[16] S. P. Dimaio, S. E. Salcudean, C. Reboulet, S. Tafazoli, K. H. Zaad. A virtual excavator for controller development and evaluation. In *Proceedings of IEEE International Conference on Robotics and Automation*, IEEE, vol. 1, pp. 52–58, 1998.

[17] T. Ni, D. X. Zhao, H. Yamada, S. Ni. A low-cost solution for excavator simulation with realistic visual effect. In *Proceedings of IEEE Conference on Robotics, Automation and Mechatronics*, IEEE, pp. 889–894, 2008.

[18] Y. Sakaida, D. Chugo, H. Yamamoto, H. Asama. The analysis of excavator operation by skillful operator — Extraction of common skills. In *Proceedings of SICE Annual Conference*, IEEE, Japan, pp. 538–542, 2008.

[19] J. Velagic, B. Lacevic, N. Osmic. Nonlinear motion control of mobile robot dynamic model, *Mobile Robots Motion Planning, New Challenges*, I–Tech., Vienna, pp. 531–552, 2008.

[20] B. Lacevic, J. Velagic, B. Perunicic. Reduction of control torques of mobile robot using hybrid nonlinear position controller. In *Proceedings of International Conference on Computer as a Tool*, IEEE, Serbia & Montenegro, Belgrade, Sylvie, vol. 1, pp. 314–317, 2005.

[21] H. Yu. Robust combined adaptive and variable structure adaptive control of robot manipulators. *Robotica*, vol. 16, no. 6, pp. 623–650, 1998.

[22] T. V. Alekseeva, K. A. Artem′ev, A. A. Bromberg, R. L. Voitsekhovskii, N. A. Ul′yanov. *Machines for Earthmoving Work: Theory and Calculations*, 1986.

[23] M. S. Hasan, H. Yu, A. Carrington, T. C. Yang. Co-simulation of wireless networked control systems over mobile ad hoc network using SIMULINK and OPNET. *IET Communications*, vol. 3, no. 8, pp. 1297–1310, 2009.

[24] M. S. Hasan, H. Yu, A. Griffiths, T. C. Yang. Interactive co-simulation of MATLAB and OPNET for Networked Control Systems. In *Proceedings of the 13th International Conference on Automation and Computing*, Stafford, UK, pp. 237–242, 2007.

[25] K. Fall, K. Varadhan. The *ns* Manual (formerly *ns* Notes and Documentation), The VINT project, [Online], Available: http://www.isi.edu/nsnam/ns/doc/ns_doc.pdf, May 9, 2010.

[26] S. Y. Han, N. B. Abu-Ghazaleh. On the Effect of Fading on Ad-hoc Networks, [Online], Available: http://arxiv.org/PS_cache/cs/pdf/0504/0504002v1.pdf, April 1, 2005.

[27] C. E. Perkins. *Ad Hoc Networking*, Boston, USA: Addison-Wesley, 2001.

[28] D. B. Johnson, D. A. Maltz, J. Broch. *Ad Hoc Networking*, Boston, USA: Addison-Wesley, 2001.

[29] F. De Pellegrini, D. Miorandi, S. Vitturi, A. Zanella. On the use of wireless networks at low level of factory automation systems. *IEEE Transactions on Industrial Informatics*, vol. 2, no. 2, pp. 129–143, 2006.

[30] Lucent Technologies Inc. ORiNOCO PC Card, Home, Office, and Public Mobile Broadband Internet Access, [Online], Available: http://www.a1datacom.com/pdf/wavelan_PC.pdf, July 2009.

[31] M. Conti, S. Giordano. Multihop ad hoc networking: The theory. *IEEE Communications Magazine*, vol. 45, no. 4, pp. 76–86, 2007.

[32] K. Goldberg, S. Gentner, C. Sutter, J. Wiegley. The mercury project: A feasibility study for internet robots. *IEEE Robotics and Automation Magazine*, vol. 7, no. 1, pp. 35–40, 2000.

[33] P. X. Liu, M. Meng, X. Ye, J. Gu. An UDP-based protocol for internet robots. In *Proceedings of the 4th World Congress on Intelligent Control and Automation*, IEEE, PRC, vol. 1, pp. 59–65, 2002.

[34] N. J. Ploplys, P. A. Kawka, A. G. Alleyne. Closed-loop control over wireless networks. *IEEE Control Systems Magazine*, vol. 24, no. 3, pp. 58–71, 2004.

[35] J. Liu, Y. Yuan, D. M. Nicol, R. S. Gray, C. C. Newport, D. Kotz, L. F. Perrone. Simulation validation using direct execution of wireless ad-hoc routing protocols. In *Proceedings of the 18th Workshop on Parallel and Distributed Simulation*, ACM, Kufstein, Austria, pp. 7–16, 2004.

[36] C. Newport. Simulating Mobile Ad Hoc Networks: A Quantitative Evaluation of Common MANET Simulation Models, Technical Report TR2004-504, Dartmouth College, USA, [Online], Available: http://cmc.cs.dartmouth.edu/cmc/papers/newport:thesis.pdf, 2004.

[37] W. Zhang, M. S. Branicky, S. M. Phillips. Stability of networked control systems. *IEEE Control Systems Magazine*, vol. 21, no. 1, pp. 84–99, 2001.

[38] J. Colandairaj, G. W. Irwin, W. G. Scanlon. An integrated approach to wireless feedback control. In *Proceedings of UKACC International Control Conference*, Glasgow, UK, 2006.

[39] N. J. Ploplys. Wireless Feedback Control of Mechanical Systems, M. Sc. dissertation, Department of Mechanical Engineering, University of Illinois, Champaign, USA, 2003.

[40] S. Zampieri. Trends in networked control systems. In *Proceedings of the 17th International Federation of Automatic Control World Congress*, Seoul, Korea, pp. 2886–2894, 2008.

[41] J. Nilsson. Real-time Control Systems with Delays, Ph. D. dissertation, Department of Automatic Control, Lund Institute of Technology, Lund, Sweden, [Online], Available: http://www.control.lth.se/documents/1998/nilj98dis.pdf, 1998.

[42] D. Henriksson. Flexible Scheduling Methods and Tools for Real Time Control Systems, Ph. D. dissertation, Department of Automatic Control, Lund Institute of Technology, Lund, Sweden, [Online], Available: http://www.control.lth.se/documents/2003/hen03.pdf, 2003.

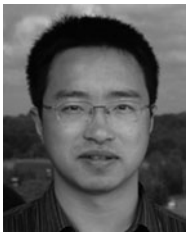

Yang Liu received the B. Eng. degree in automation from Hunan University, PRC in 2003, and the M. Sc. degree in control systems from The University of Sheffield, UK in 2005, and the Ph. D. degree in robotics from Staffordshire University, UK in 2010. He is currently a research fellow with the Centre for Applied Dynamics Research, School of Engineering, the University of Aberdeen, UK.

His research interests include control of underactuated systems, mobile robots, and mechatronics.

E-mail: y.liu@staffs.ac.uk (Corresponding author)

Mohammad Shahidul Hasan received the B. Sc. and first M. Sc. degrees in computer science from the University of Dhaka, Bangladesh. He received the second M. Sc. degree in computer and network engineering from Sheffield Hallam University, UK. He has been awarded a Ph. D. degree at Staffordshire University, UK in networked control systems over mobile ad-hoc network (MANET). He worked as a assistant professor in the Department of Computer Science and Engineering at the University of Dhaka in Bangladesh. Currently, he is a lecturer at Staffordshire University.

His research interests include computer networks, networked control systems, and remotely controllable mobile robot systems.

E-mail: m.s.hasan@staffs.ac.uk

Hong-Nian Yu has held academic positions at the Universities of Yanshan, Sussex, Liverpool John Moor, Exeter, Bradford, and Staffordshire. He is currently a professor of computer science and the director of Mobile Fusion Applied Research Centre at Staffordshire University, UK.

He research interests include modelling and control of robots and mechatronics devices and neural networks, mobile computing, modelling, scheduling, planning and simulations of large discrete event dynamic systems, radio frequency identification (RFID) with applications to manufacturing systems, supply chains, transportation networks, and computer networks.

E-mail: h.yu@staffs.ac.uk